Supplementary Materials

In situ X-ray Diffraction Computed Tomography studies examining the thermal and chemical stabilities of working $Ba_{0.5}Sr_{0.5}Co_{0.8}Fe_{0.2}O_{3-\delta}$ membranes during oxidative coupling of methane

Dorota Matras[1,2*], Antonis Vamvakeros[2,3,4] Simon D. M. Jacques[3*], Vesna Middelkoop[5], Gavin Vaughan[6], Robert J. Cernik[1] and Andrew M. Beale[2,3,4*]

[1] School of Materials, University of Manchester, Manchester, Lancashire M13 9PL, UK
[2] Research Complex at Harwell, Harwell Science and Innovation Campus, Rutherford Appleton Laboratory, Didcot, Oxon, OX11 0FA, UK.
[3] Finden Limited, Merchant House, 5 East St Helen Street, Abingdon, OX14 5EG, UK.
[4] Department of Chemistry, University College London, 20 Gordon Street, London, WC1H 0AJ, UK.
[5] Sustainable Materials Management, Flemish Institute for Technological Research, VITO NV, Boeretang 200, Mol, Belgium
[6] ESRF- The European Synchrotron, Grenoble, 38000 France.
* Correspondence: matras.dorota@gmail.com (D.M.); simon@finden.ac.uk (S.D.M.J.); andrew.beale@ucl.ac.uk (A.M.B.)

S1. Experimental setup

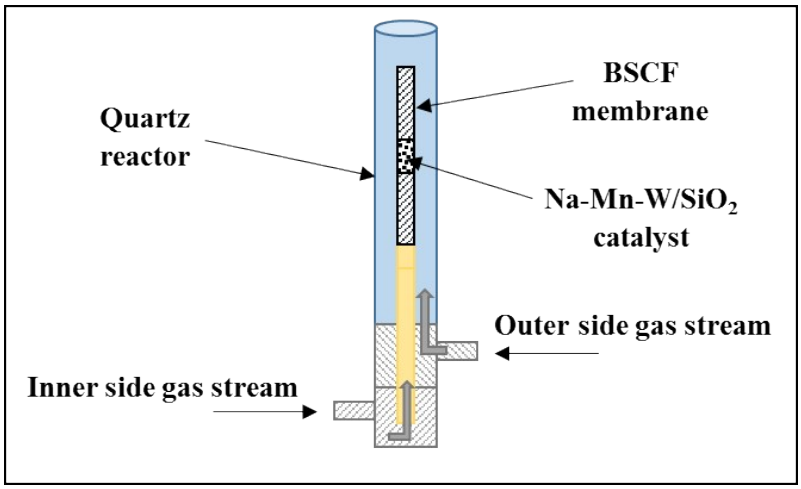

Figure S1. Schematic representation of the experiment cell. The inner side gas is delivered to the membrane using two nonporous alumina tubes, connected to each other and to the BSCF membrane with ceramic adhesive (Ceramabond™). The gas delivery stub (grey-lined area) was made from brass and a Swagelok union tee. The entire gas delivery setup was gastight and graphite ferrules were used in order to prevent the inner and outer side gas streams from mixing.

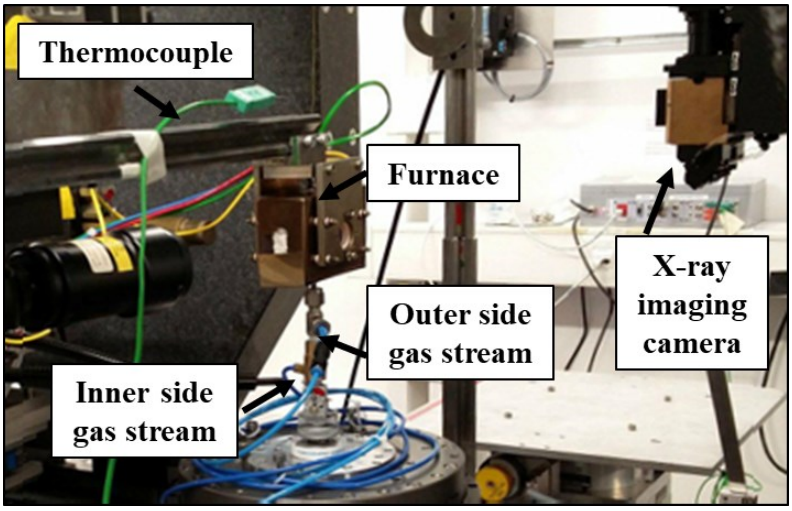

Figure S2. Photograph of experimental set up at the ID15A beamline.

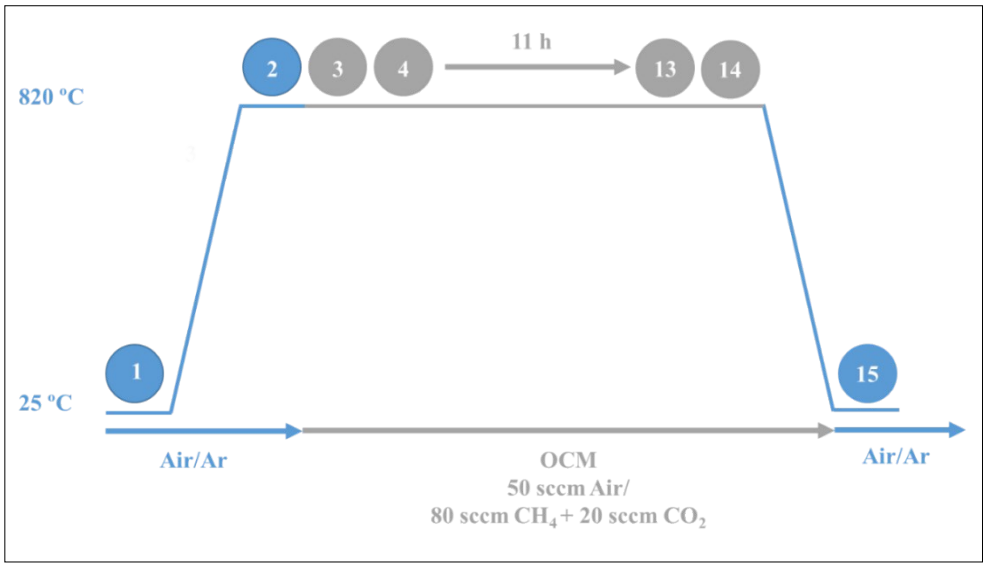

Figure S3. Schematic representation of the protocol used for the catalytic membrane reactor experiment at ID15A, ESRF. Numbers correspond to XRD-CT scan number.

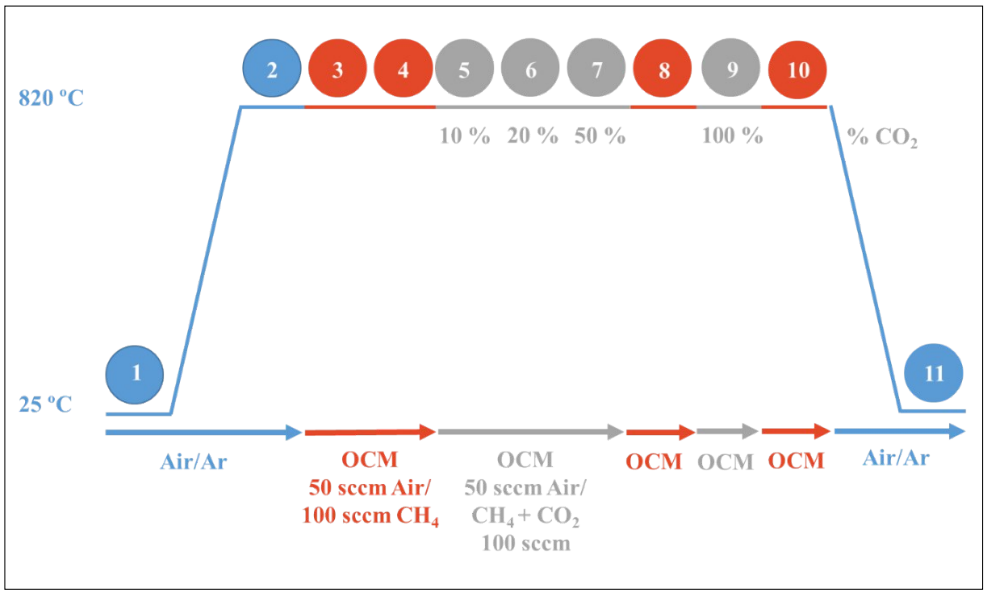

Figure S4. Schematic representation of the protocol used for the packed-bed catalytic membrane reactor experiment at ID15A, ESRF. Numbers correspond to XRD-CT scan number.

Table S1. Phases identified and used in the analysis of XRD-CT data.

Phase	Crystallographic details	ICSD/PDF database code	Reflections in 2Th (95 kev)/d spacing (Å)
	Membrane material		
Co_3O_4	cubic, *Fd-3m*	28158	
CoO	cubic, *Fm-3m*	9865	
$Ba_6Co_4O_{12}$	hexagonal, $P6_3/mcm$	00-048-1773	
	hkl_phase/peak phase		
BSCF	cubic, P*m-3m*	109462	
BSCF 001			1.875 (4.009)
BSCF 011			2.651 (2.836)
BSCF 111			3.246 (2.316)
BSCF 002			3.747 (2.006)
BSCF 021			4.189 (1.795)
BSCF 211			4.589 (1.639)
BSCF 022			5.299 (1.419)
Unknown I1			1.825 (4.107)
Unknown I2			2.238 (3.365)
Unknown I3			2.890 (2.596)
Unknown I4			3.421 (2.196)
Unknown I5			3.655 (2.055)
	Catalyst material		
Cristobalite			3.013
Tridymite			1.754
Na_2WO_4			1.418
Mn_2O_3			2.763
$BaWO_4$			2.283
$MnWO_4$			2.505

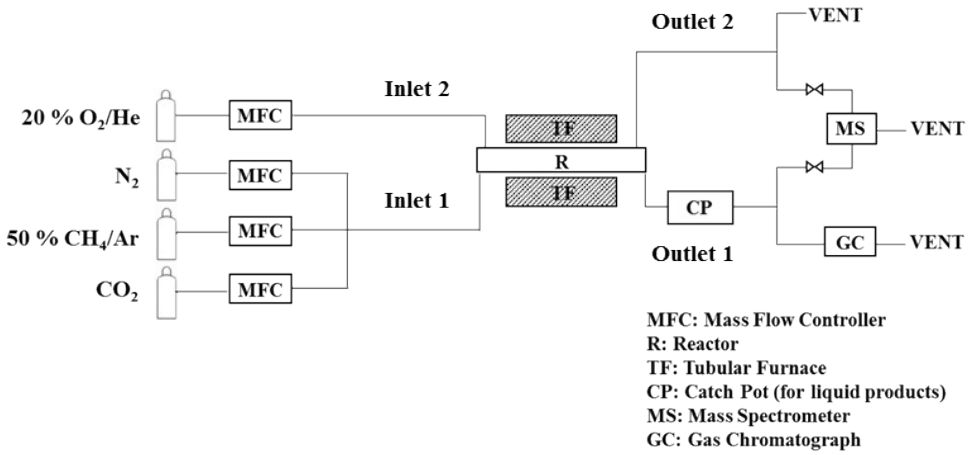

Figure S5. Schematic representation of laboratory experimental set up.

Table S2. Experimental protocol for the laboratory measurements with the catalytic membrane reactor.

Measurement stage	Conditions
Temperature ramp (820 °C)	20 % O_2/He (outer side), N_2 (inner side)
OCM	100 sccm of 20 % O_2/He; 100 sccm of CH_4
20 % CO_2/OCM	100 sccm of 20 % O_2/He; 80 sccm of CH_4 and 20 sccm of CO_2
OCM	100 sccm of 20 % O_2/He; 100 sccm of CH_4
20 % CO_2/OCM	100 sccm of 20 % O_2/He; 80 sccm of CH_4 and 20 sccm of CO_2
Cooling to 25 °C	N_2

Table S3. Experimental protocol for the laboratory measurements with packed-bed catalytic membrane reactor.

Measurement stage	Conditions
Temperature ramp (820 °C)	20 % O_2/He (outer side), N_2 (inner side)
OCM	104 sccm of 20 % O_2/He; 140 sccm of CH_4
10 % CO_2/OCM	100 sccm of 20 % O_2/He; 90 sccm of CH_4 and 10 sccm of CO_2
20 % CO_2/OCM	100 sccm of 20 % O_2/He; 80 sccm of CH_4 and 20 sccm of CO_2
50 % CO_2/OCM	100 sccm of 20 % O_2/He; 50 sccm of CH_4 and 50 sccm of CO_2
OCM	100 sccm of 20 % O_2/He; 100 sccm of CH_4
100 % CO_2/OCM	104 sccm of 20 % O_2/He; 70 sccm of CO_2
OCM	100 sccm of 20 % O_2/He; 100 sccm of CH_4
Cooling to 25 °C	N_2

S2. XRD-CT measurements of catalytic membrane reactor

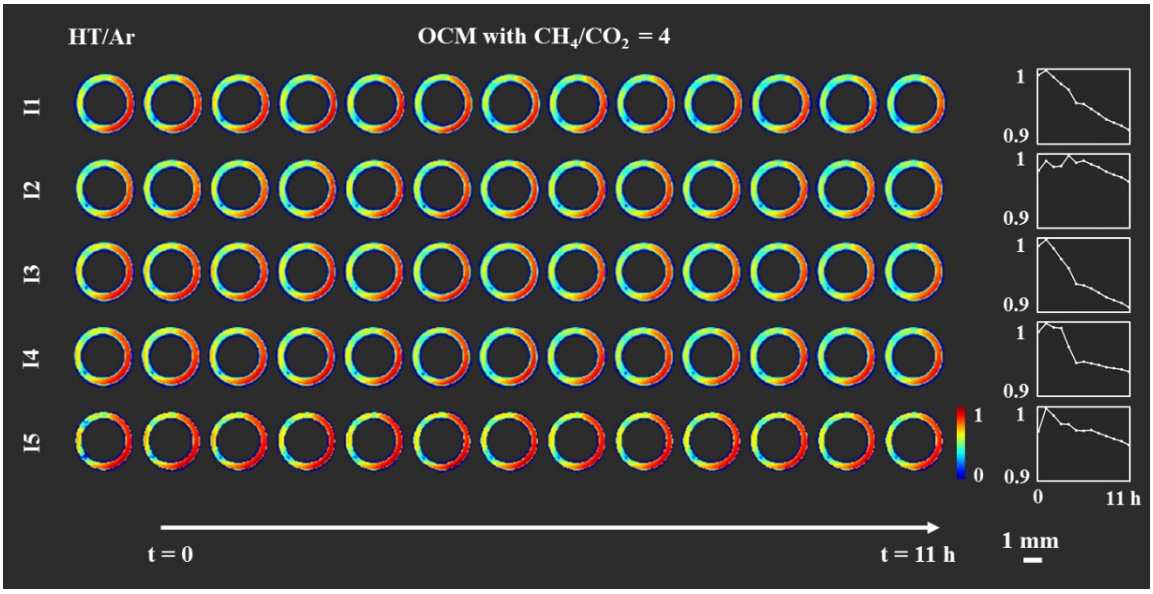

Figure S6. Distribution of unknown phase/reflections during the high temperature XRD-CT scan and OCM reaction. Plots on the right corresponds to changes in the normalised peak intensity as a function of time.

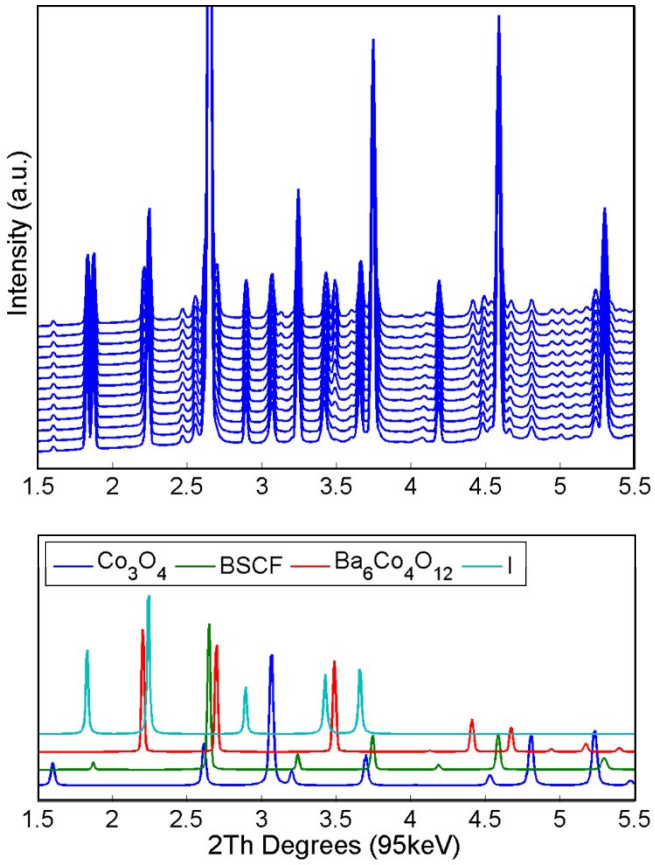

Figure S7. Top panel: Stack of the mean diffraction patterns exported from the 13 XRD-CT datasets collected under high temperature scans and OCM reaction conditions (bottom: Ar flow, top: after 11 hr of OCM with CH_4/CO_2 = 4). Bottom panel: Simulated diffraction patterns for the various crystalline components present in the membrane material at high temperatures.

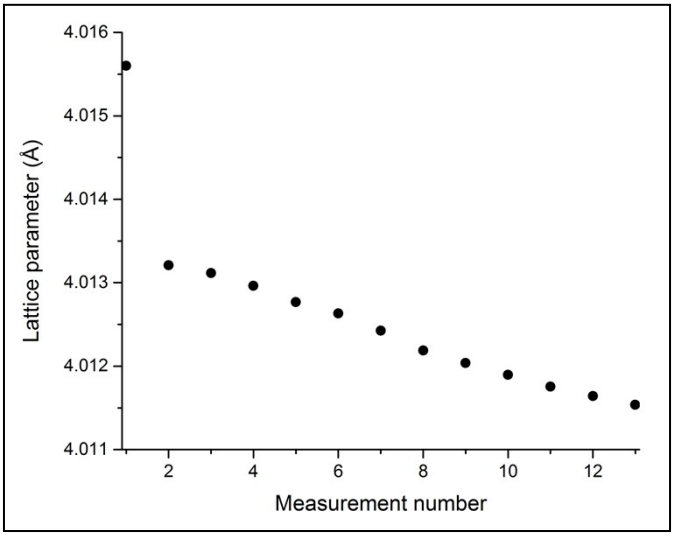

Figure S8. Changes in the lattice parameter of cubic BSCF as a function of time at high temperature; each XRD-CT scan was acquired 1 hr apart. First scan was acquired under Ar flow and the following ones under OCM with CH_4/CO_2 = 4. The most significant change from in lattice parameter from 4.0155 to 4.0132 Å was observed when introducing the OCM reaction mixture.

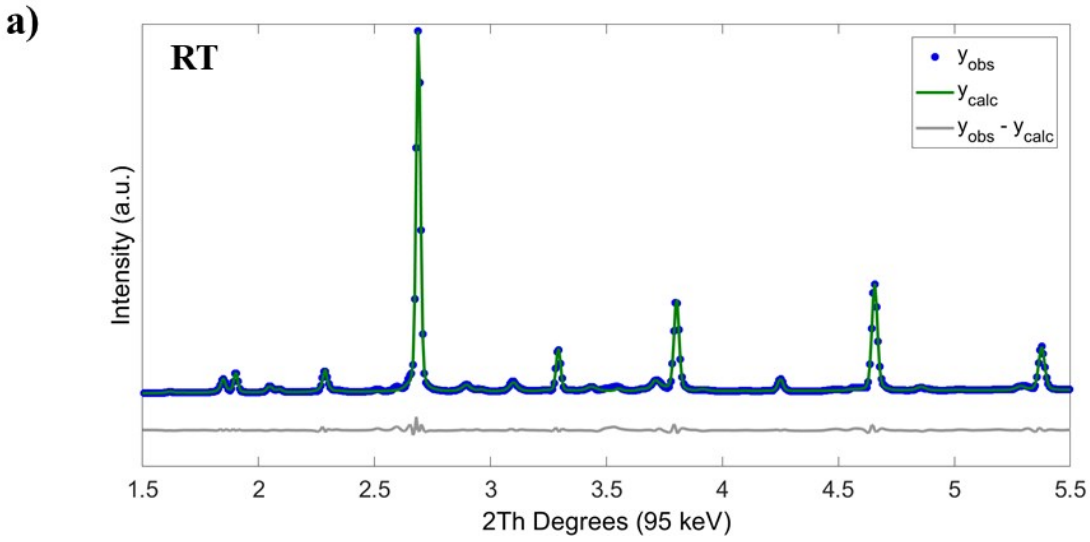

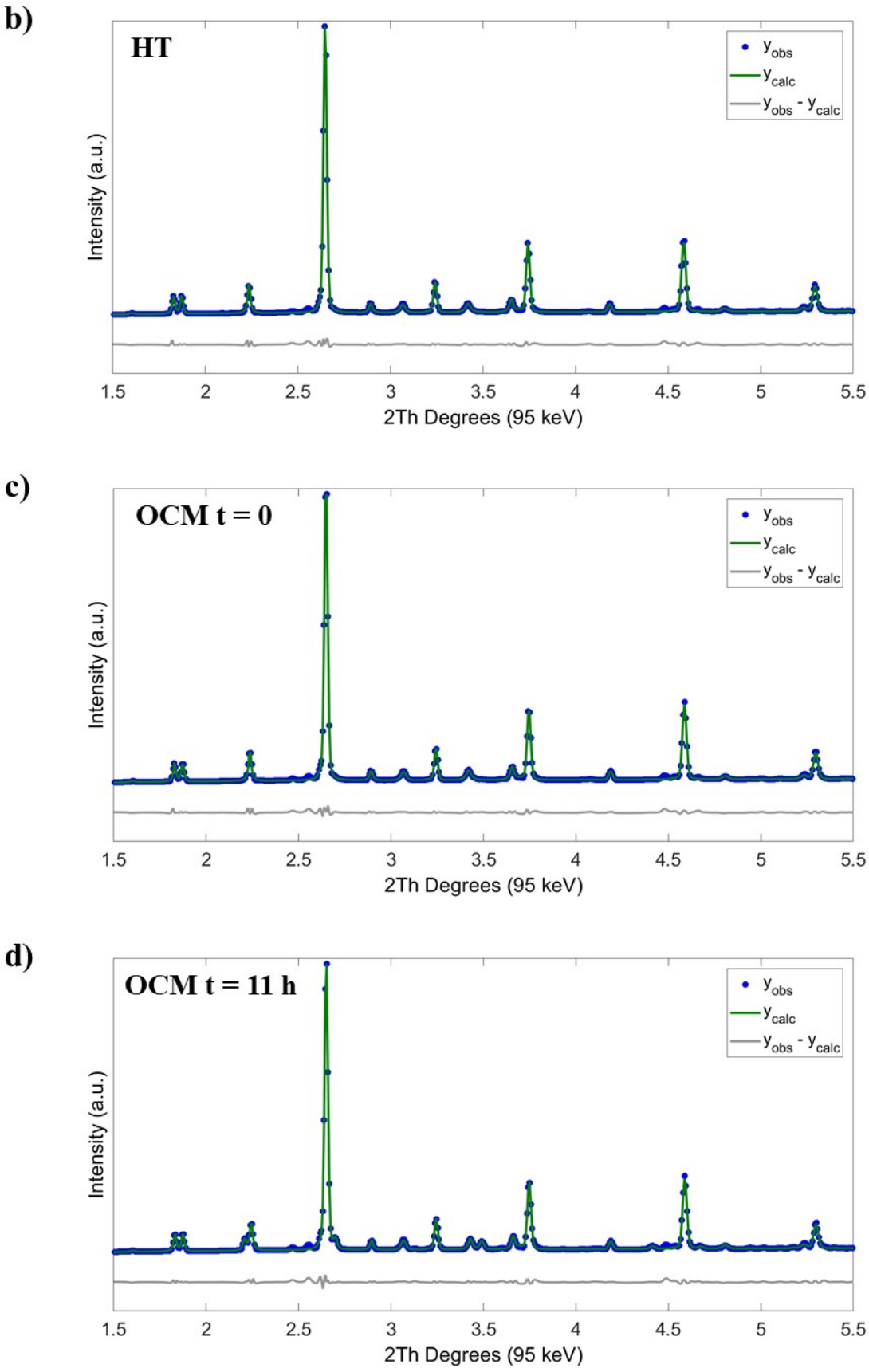

Figure S9. Fits from the full profile analysis of the mean diffraction patterns from four selected XRD-CT datasets from the first CMR experiment: a) scan at room temperature of the fresh membrane, b) scan at

high temperature after Ar treatment, c) first scan under OCM reaction conditions and d) last scan under OCM reaction conditions.

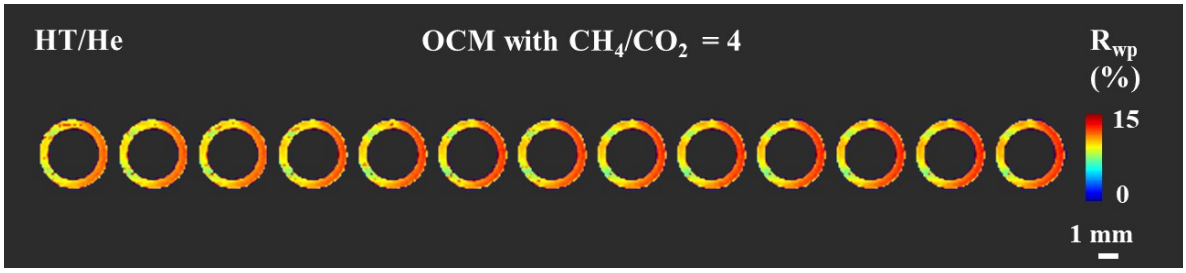

Figure S10. Distribution of Rwp for all high temperature XRD-CT measurements. The error is relatively uniform with a small % increase in the areas where the secondary phases are primarily located.

S3. Simulation of BSCF diffraction patterns

The simulated BSCF diffraction patterns were created using the Topas v5 software and the BSCF #109462 structure from the ICSD database. The aim of these simulations was to understand how the relative intensity of various reflections change when we vary the composition at the A site, B site and oxygen deficiency. When investigating the composition of A site, the occupancy of Ba was varied between 0.2 and 0.8 and the occupancy of Sr was altered accordingly so that the occupancy of both elements together at the A site was equal to 1. This approach allowed us to calculate the new diffraction pattern and investigate the relative changes in intensity of the various reflections. The same approach was also used for the Co and Fe present at the B site. Regarding the O deficiency, the oxygen occupancy varied between 0.8 and 1 but the composition of the A and B site was kept constant. Decreasing the oxygen occupancy should lead to a change in the oxidation state of elements at the A and B site in order to maintain the charge neutrality of the system, however in this simulation we decided not to account for these changes as it would lead to a complex structure and the aim here is to observe the general trend in the relative peak intensities.

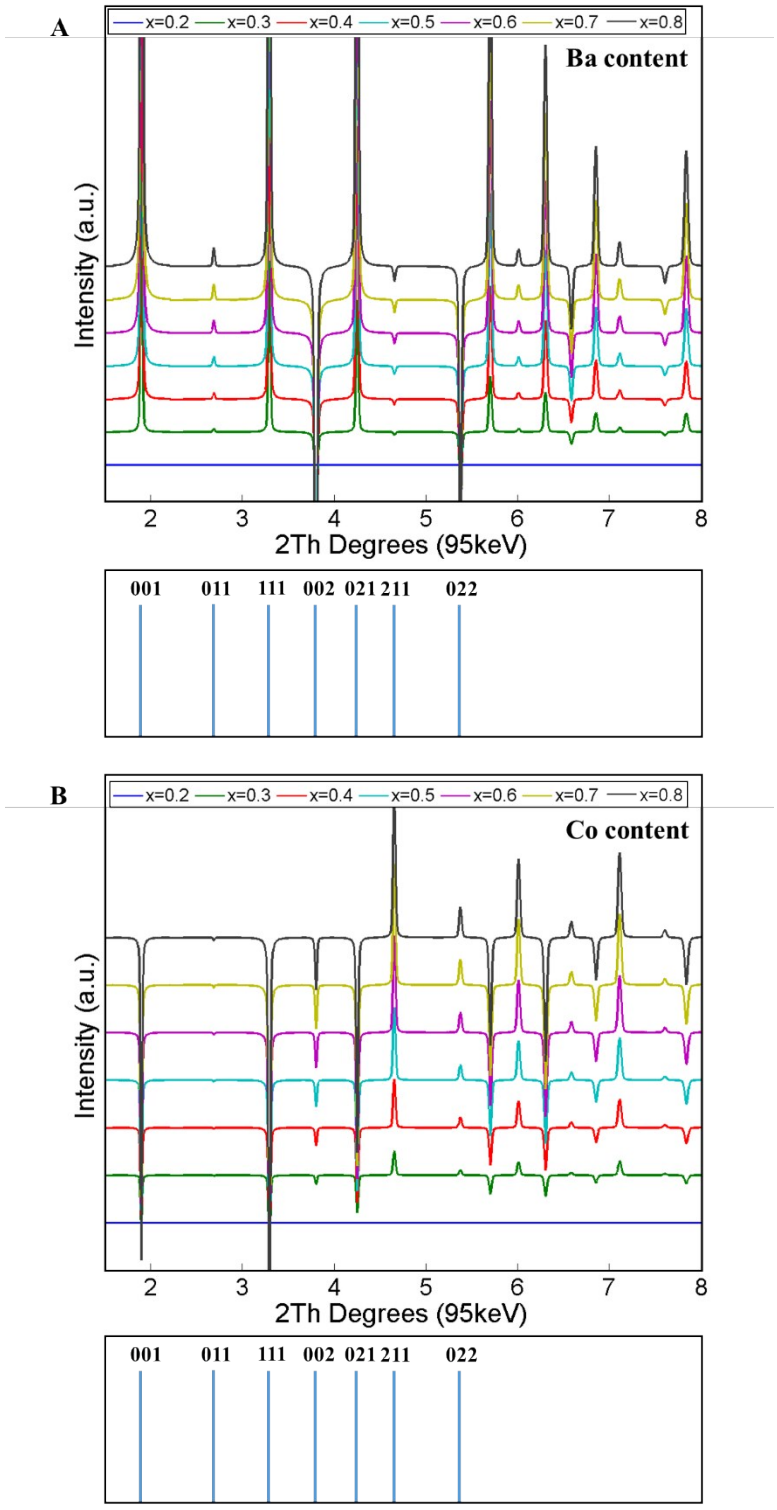
A
x=0.2
x=0.3
x=0.4
x=0.5
x=0.6
x=0.7
x=0.8
Ba content
Intensity (a.u.)
2
3
4
5
6
7
8
2Th Degrees (95keV)
001
011
111
002
021
211
022
B
x=0.2
x=0.3
x=0.4
x=0.5
x=0.6
x=0.7
x=0.8
Co content
Intensity (a.u.)
2
3
4
5
6
7
8
2Th Degrees (95keV)
001
011
111
002
021
211
022

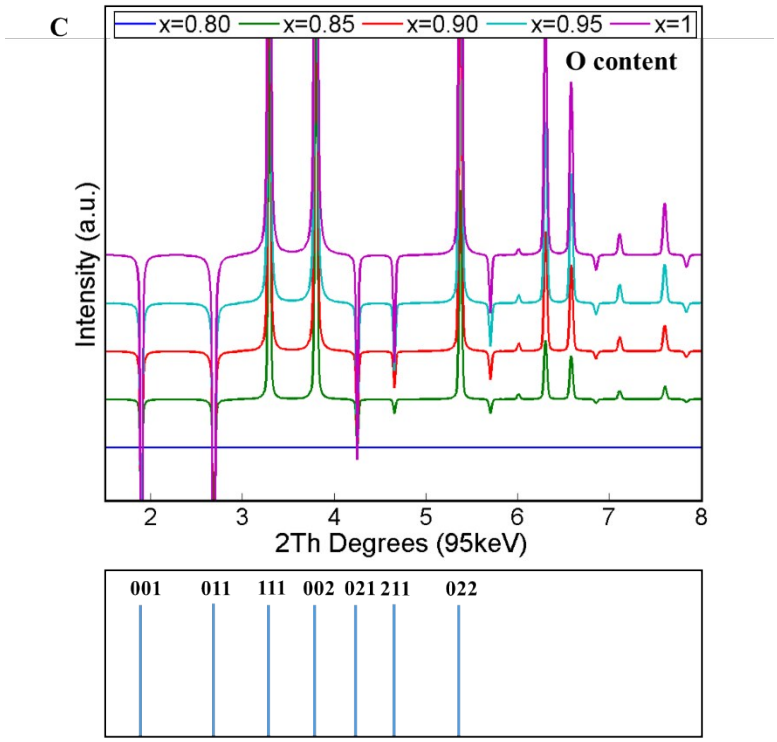

Figure S11. Simulated diffraction patterns of cubic BSCF structure varying the content of A) Ba in $Ba_xSr_{1-x}Co_{0.8}Fe_{0.2}O_3$, B) Co in $Ba_{0.5}Sr_{0.5}Co_xFe_{1-x}O_3$ and C) O in $Ba_{0.5}Sr_{0.5}Co_{0.8}Fe_{0.2}O_x$.

Table S4. Comparison between the observed and simulated diffraction patterns

Reflection	Observed	Structural changes obtained with simulations		
		O_{occ}	Co_{occ}	Ba_{occ}
001	↓	↑	↑	↓
011	↑	↓	↓	↑
111	↑	↑	↓	↑
002	↑	↑	↓	↓
021	↓	↑	↑	↓
211	↑	↓	↑	↓
022	↑	↑	↑	↓

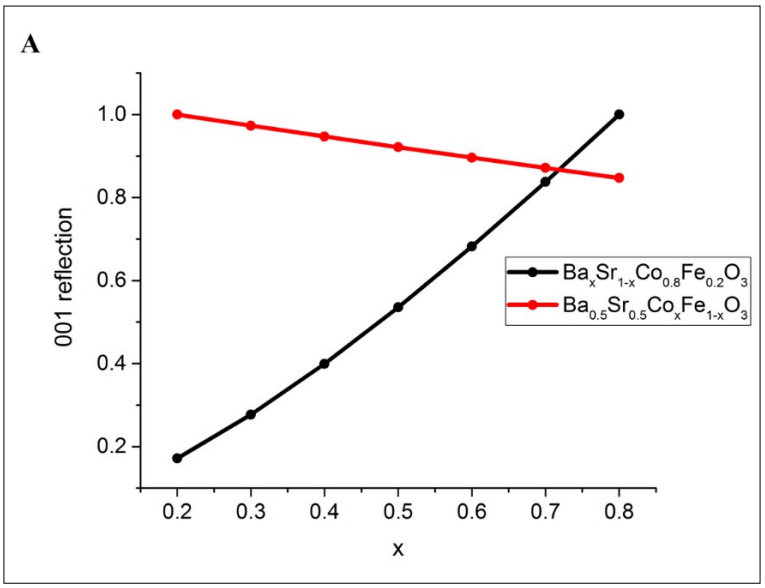
A
001 reflection
1.0
0.8
0.6
0.4
0.2
0.2
0.3
0.4
0.5
0.6
0.7
0.8
x
Ba$_x$Sr$_{1-x}$Co$_{0.8}$Fe$_{0.2}$O$_3$
Ba$_{0.5}$Sr$_{0.5}$Co$_x$Fe$_{1-x}$O$_3$

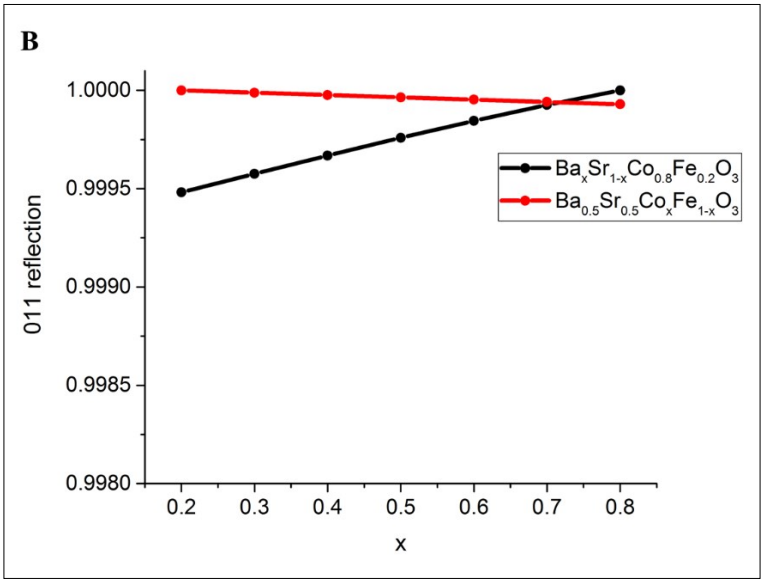
B
011 reflection
1.0000
0.9995
0.9990
0.9985
0.9980
0.2
0.3
0.4
0.5
0.6
0.7
0.8
x
Ba$_x$Sr$_{1-x}$Co$_{0.8}$Fe$_{0.2}$O$_3$
Ba$_{0.5}$Sr$_{0.5}$Co$_x$Fe$_{1-x}$O$_3$

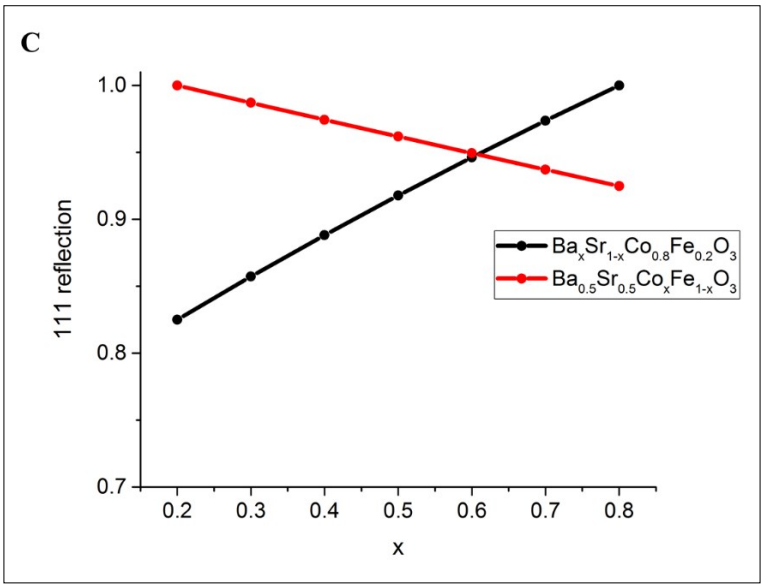
C
111 reflection
1.0
0.9
0.8
0.7
0.2
0.3
0.4
0.5
0.6
0.7
0.8
x
Ba$_x$Sr$_{1-x}$Co$_{0.8}$Fe$_{0.2}$O$_3$
Ba$_{0.5}$Sr$_{0.5}$Co$_x$Fe$_{1-x}$O$_3$

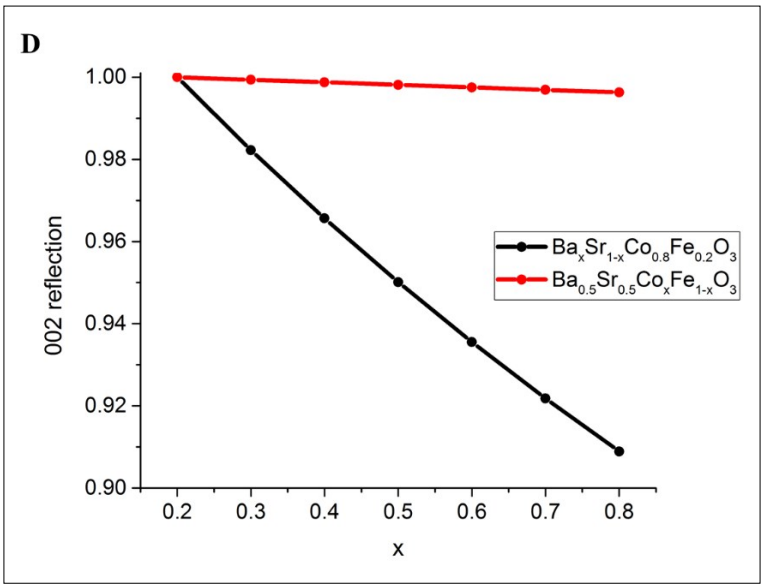
D
1.00
0.98
0.96
0.94
0.92
0.90
002 reflection
0.2
0.3
0.4
0.5
0.6
0.7
0.8
x
Ba$_x$Sr$_{1-x}$Co$_{0.8}$Fe$_{0.2}$O$_3$
Ba$_{0.5}$Sr$_{0.5}$Co$_x$Fe$_{1-x}$O$_3$

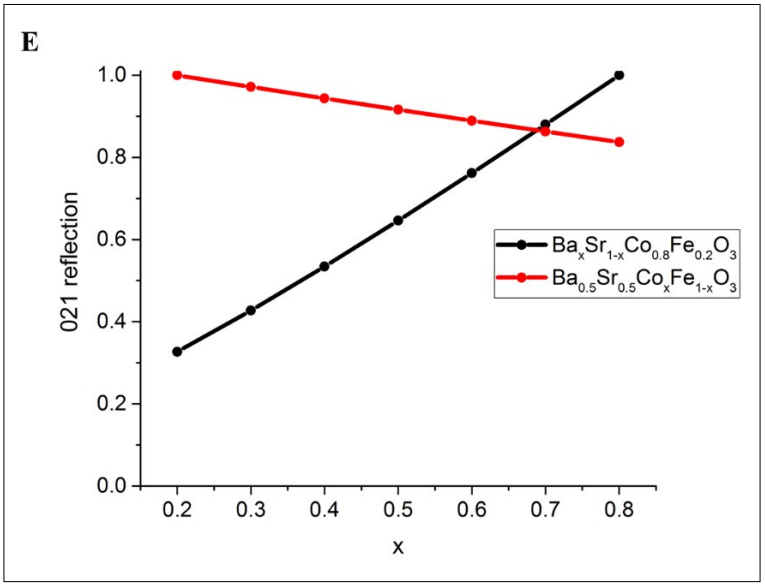
E
1.0
0.8
0.6
0.4
0.2
0.0
021 reflection
0.2
0.3
0.4
0.5
0.6
0.7
0.8
x
Ba$_x$Sr$_{1-x}$Co$_{0.8}$Fe$_{0.2}$O$_3$
Ba$_{0.5}$Sr$_{0.5}$Co$_x$Fe$_{1-x}$O$_3$

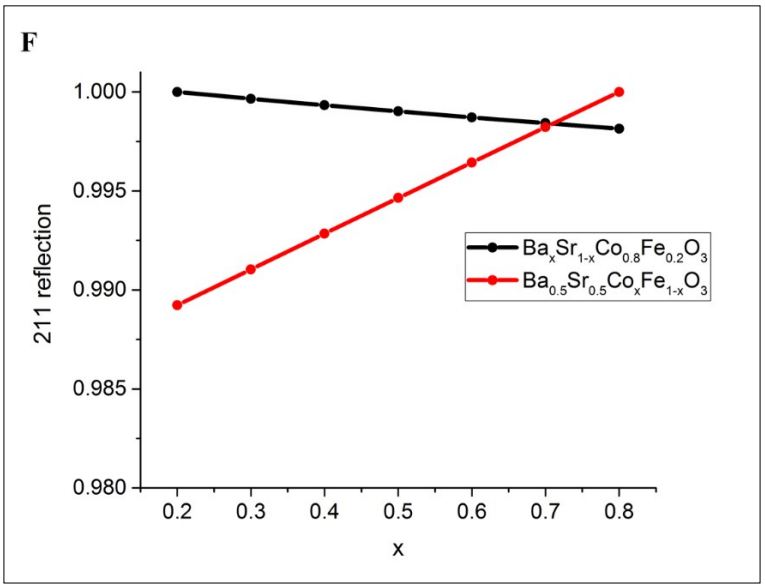
F
1.000
0.995
0.990
0.985
0.980
211 reflection
0.2
0.3
0.4
0.5
0.6
0.7
0.8
x
Ba$_x$Sr$_{1-x}$Co$_{0.8}$Fe$_{0.2}$O$_3$
Ba$_{0.5}$Sr$_{0.5}$Co$_x$Fe$_{1-x}$O$_3$

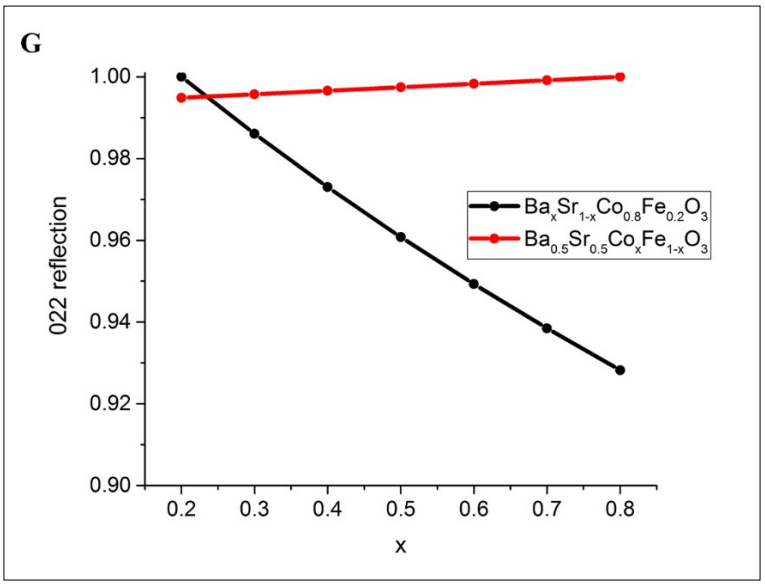

Figure S12. Normalised intensities using the summed peak intensity of various reflections A) 001, B) 011, C) 111, D) 002, E) 021, F) 211 and G) 022 from the simulated diffraction patterns of BSCF cubic structure, varying the Ba and Co content.

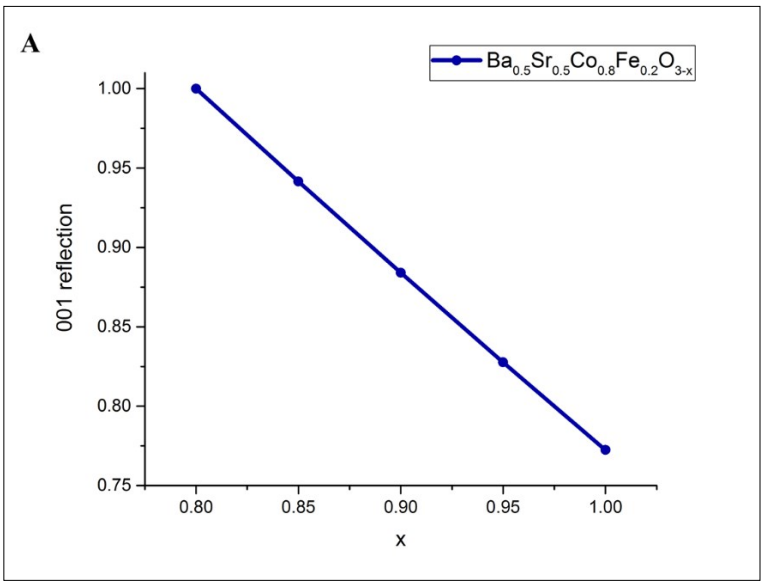

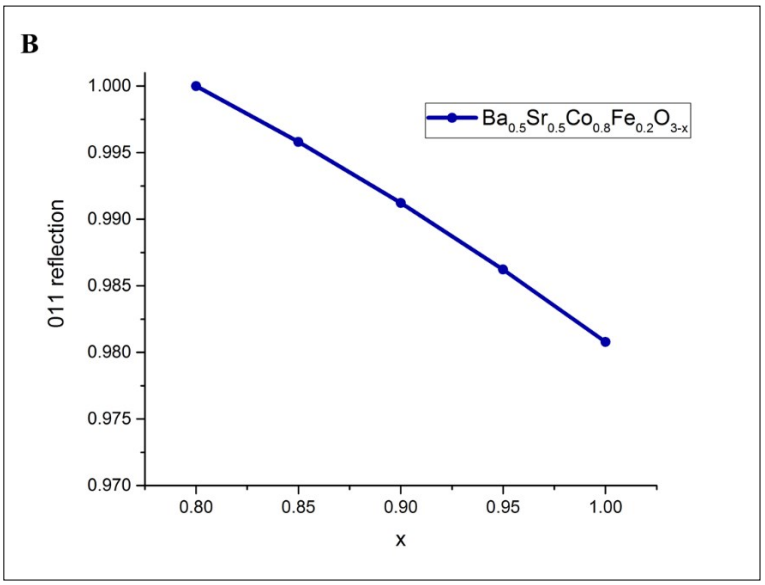
B
1.000
0.995
0.990
0.985
0.980
0.975
0.970
011 reflection
0.80
0.85
0.90
0.95
1.00
x
Ba0.5Sr0.5Co0.8Fe0.2O3-x

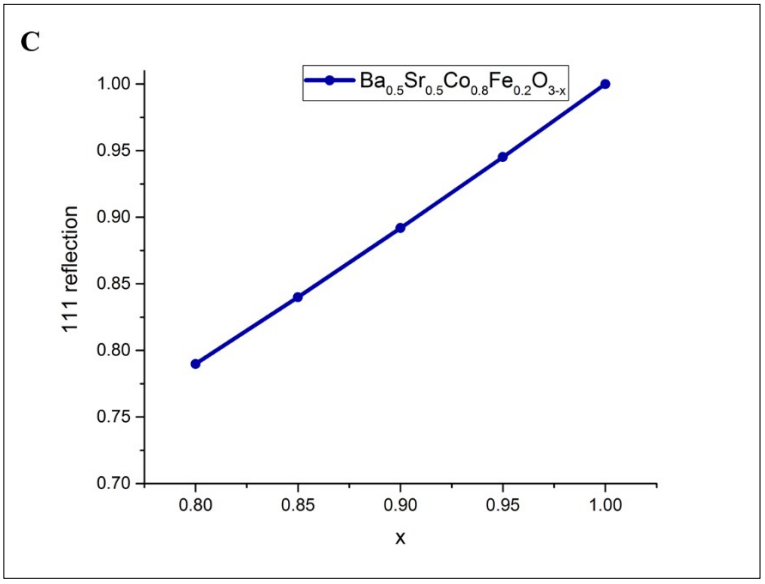
C
1.00
0.95
0.90
0.85
0.80
0.75
0.70
111 reflection
0.80
0.85
0.90
0.95
1.00
x
Ba0.5Sr0.5Co0.8Fe0.2O3-x

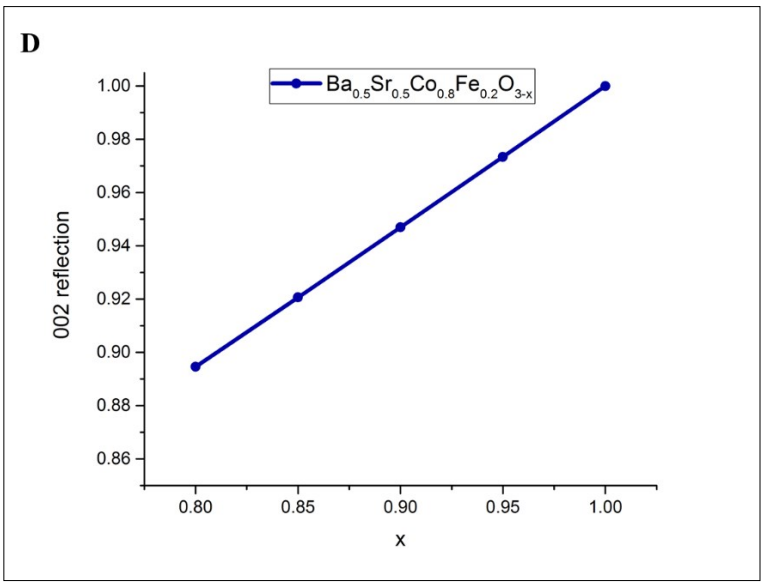
D
1.00
0.98
0.96
0.94
0.92
0.90
0.88
0.86
002 reflection
0.80
0.85
0.90
0.95
1.00
x
Ba0.5Sr0.5Co0.8Fe0.2O3-x

E

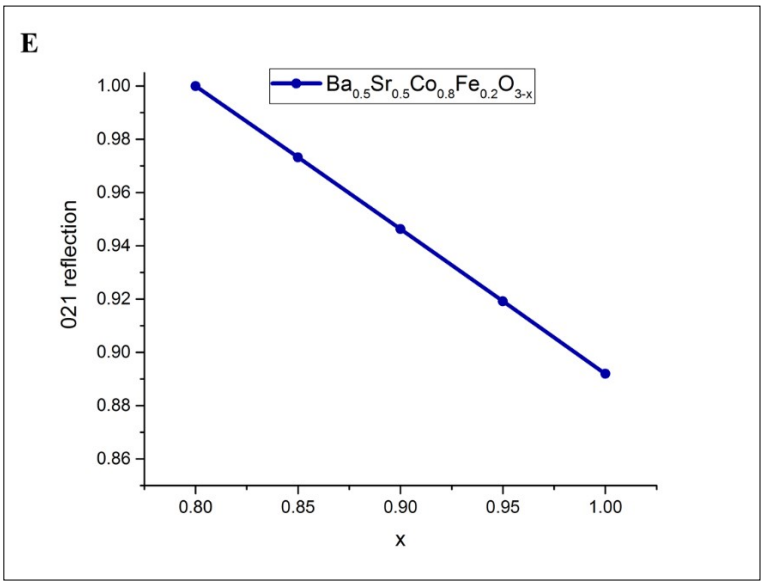
Ba0.5Sr0.5Co0.8Fe0.2O3-x
021 reflection
1.00
0.98
0.96
0.94
0.92
0.90
0.88
0.86
0.80
0.85
0.90
0.95
1.00
x

F

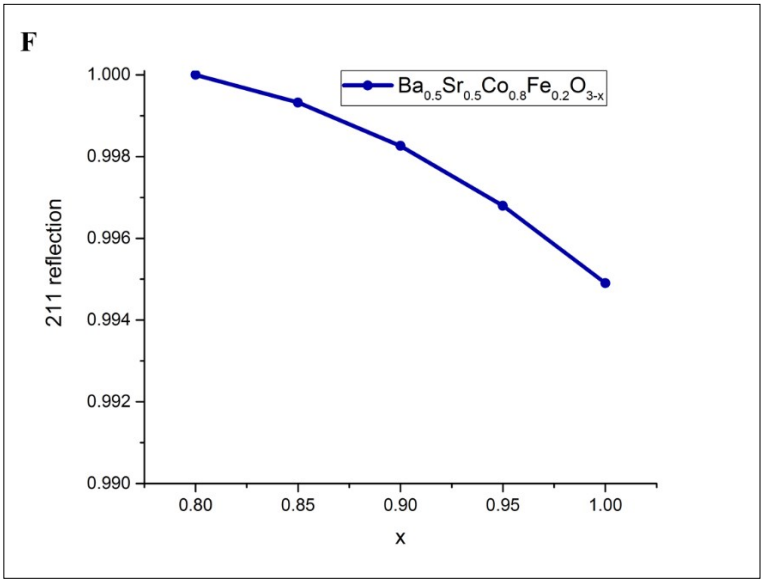
Ba0.5Sr0.5Co0.8Fe0.2O3-x
211 reflection
1.000
0.998
0.996
0.994
0.992
0.990
0.80
0.85
0.90
0.95
1.00
x

G

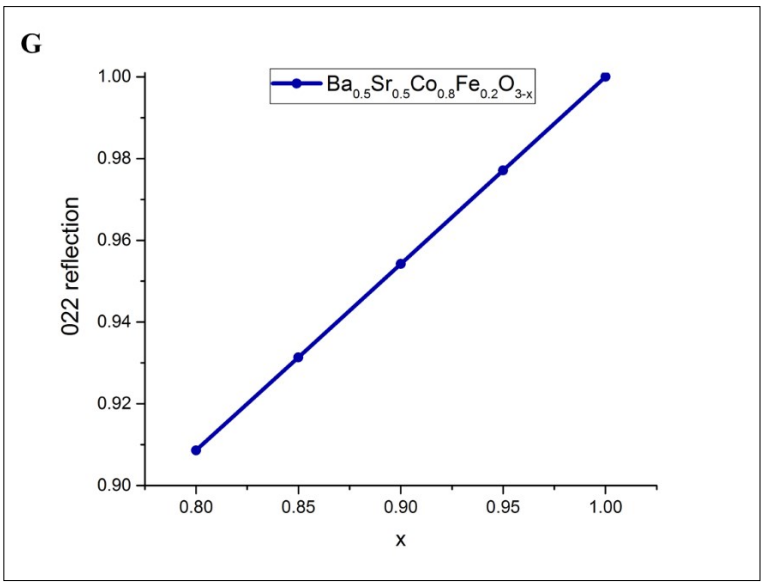
Ba0.5Sr0.5Co0.8Fe0.2O3-x
022 reflection
1.00
0.98
0.96
0.94
0.92
0.90
0.80
0.85
0.90
0.95
1.00
x

Figure S13. Normalised intensities using the summed peak intensity of various reflections A) 001, B) 011, C) 111, D) 002, E) 021, F) 211 and G) 022 from the simulated diffraction patterns of BSCF cubic structure, varying the O content.

S4. XRD-CT measurements of catalytic membrane reactor with Na-Mn-W/SiO_2 packed-bed

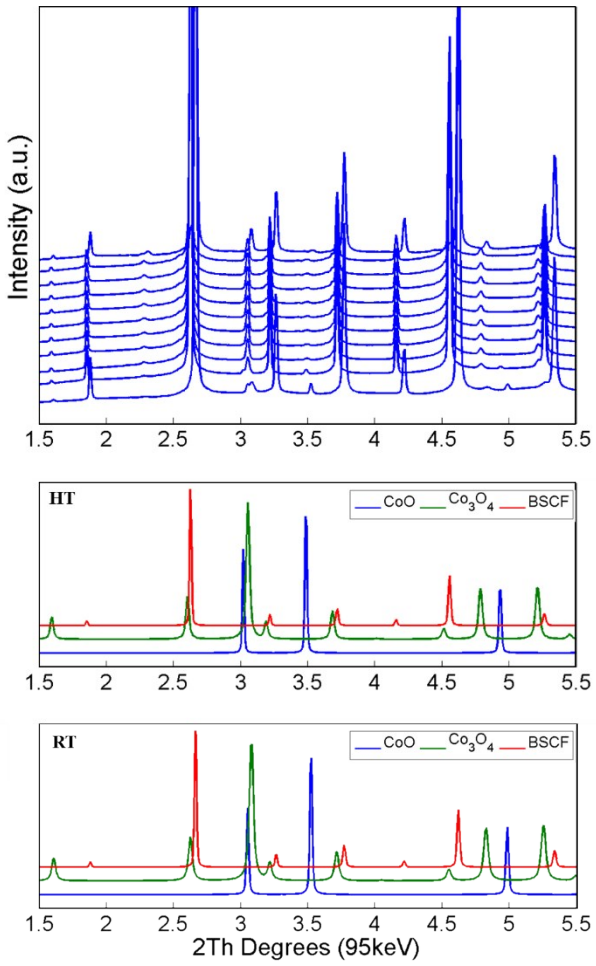

Figure S14. Top panel: Stack of the mean diffraction patterns exported from the 11 XRD-CT datasets collected during the OCM experiment (bottom: room temperature before OCM, top: room temperature after OCM). Bottom panel: Simulated diffraction patterns for crystalline components present in membrane material at room temperature and high temperature.

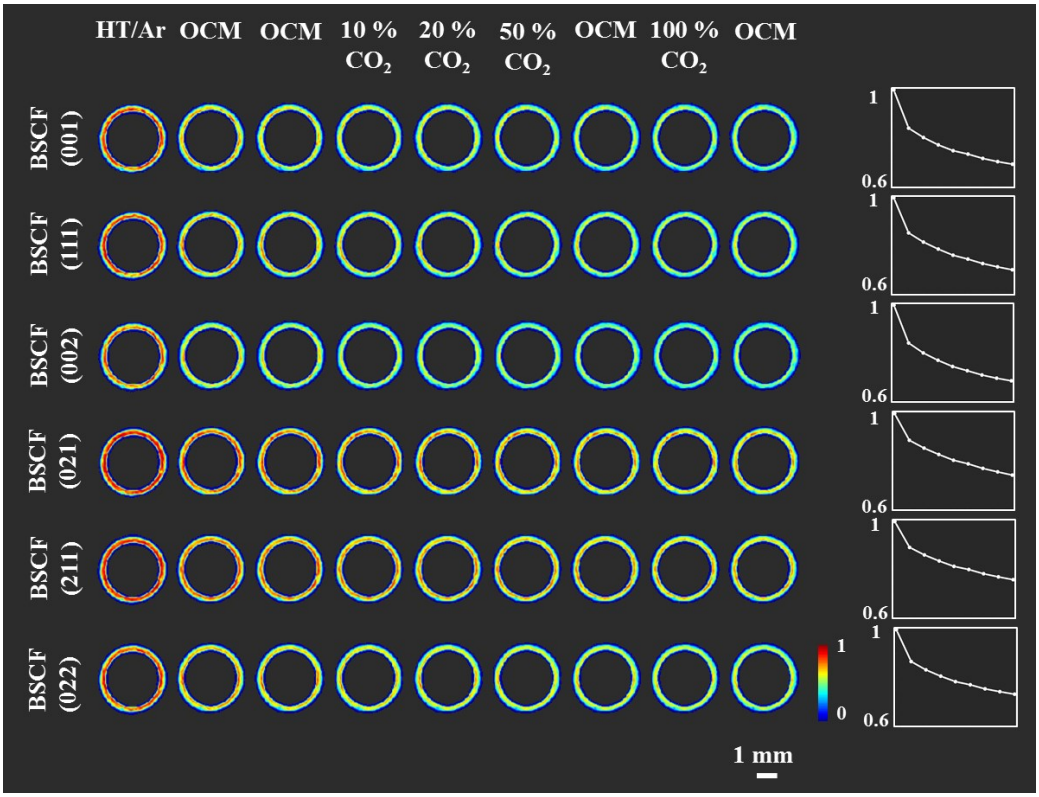

Figure S15. Distribution of the BSCF cubic perovskite reflections during the OCM experiment. Plots on the right correspond to the relative changes in the summed peak intensity.

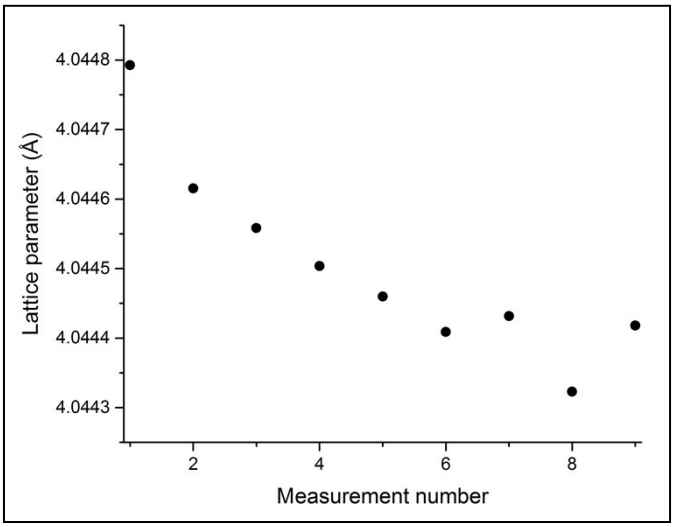

Figure S16. Changes in the lattice parameter of cubic BSCF vs. the nine XRD-CT scans collected at high temperature.

a)

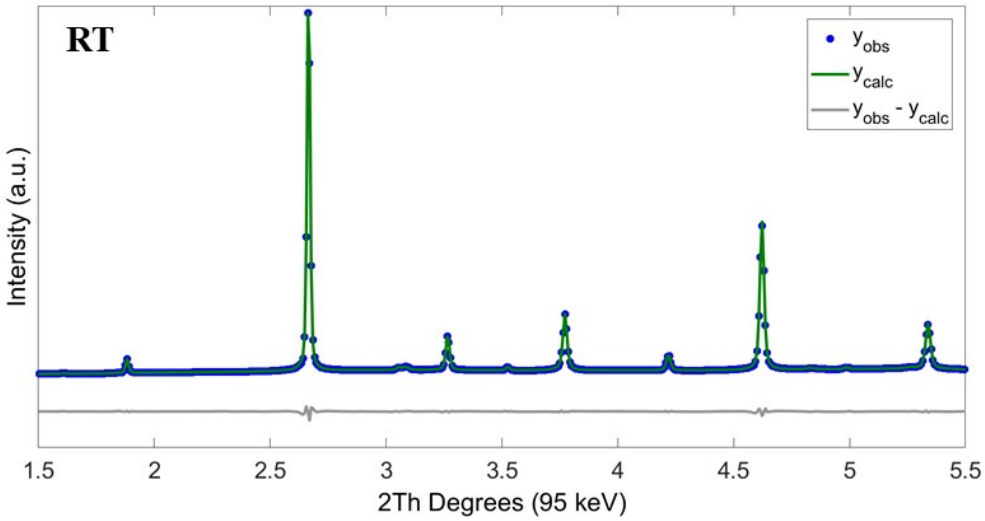
RT
y_{obs}
y_{calc}
y_{obs} - y_{calc}
Intensity (a.u.)
1.5
2
2.5
3
3.5
4
4.5
5
5.5
2Th Degrees (95 keV)

b)

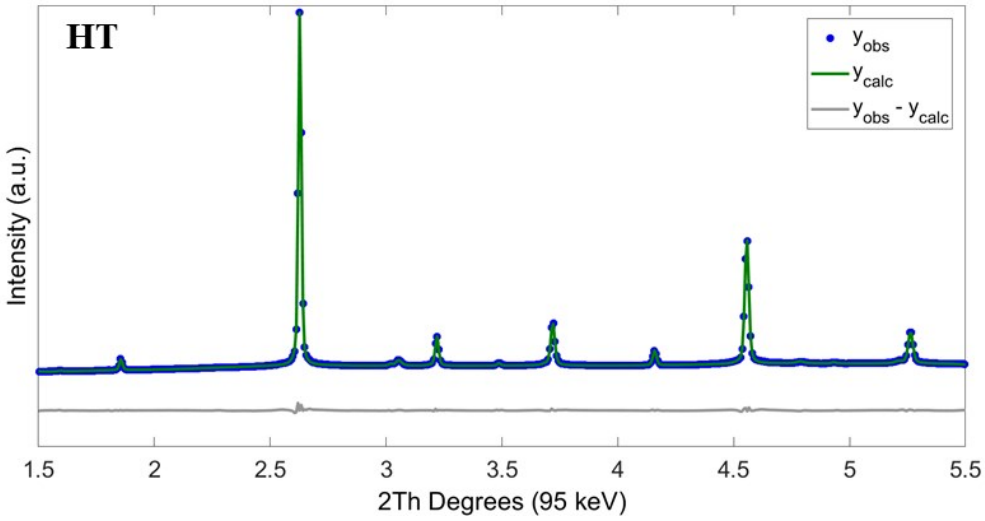
HT
y_{obs}
y_{calc}
y_{obs} - y_{calc}
Intensity (a.u.)
1.5
2
2.5
3
3.5
4
4.5
5
5.5
2Th Degrees (95 keV)

c)

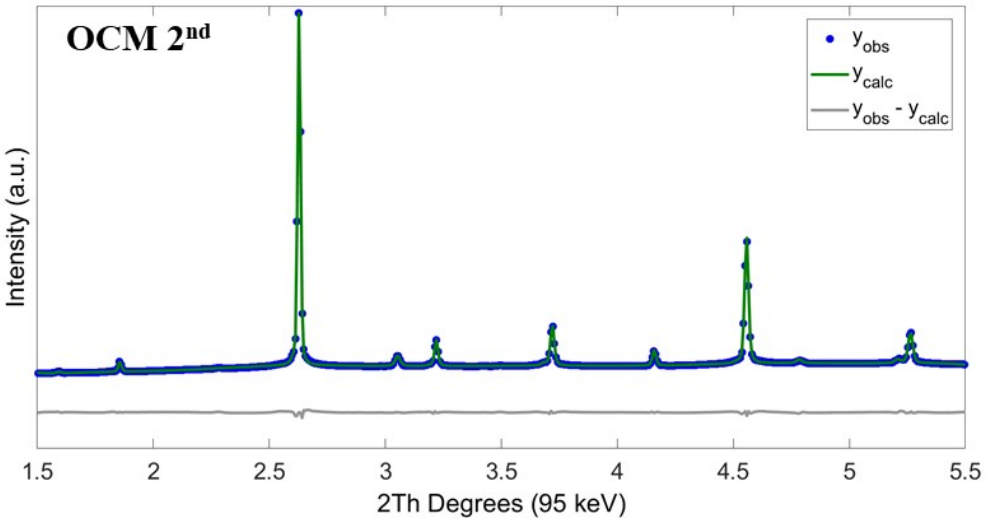
OCM 2nd
y_{obs}
y_{calc}
y_{obs} - y_{calc}
Intensity (a.u.)
1.5
2
2.5
3
3.5
4
4.5
5
5.5
2Th Degrees (95 keV)

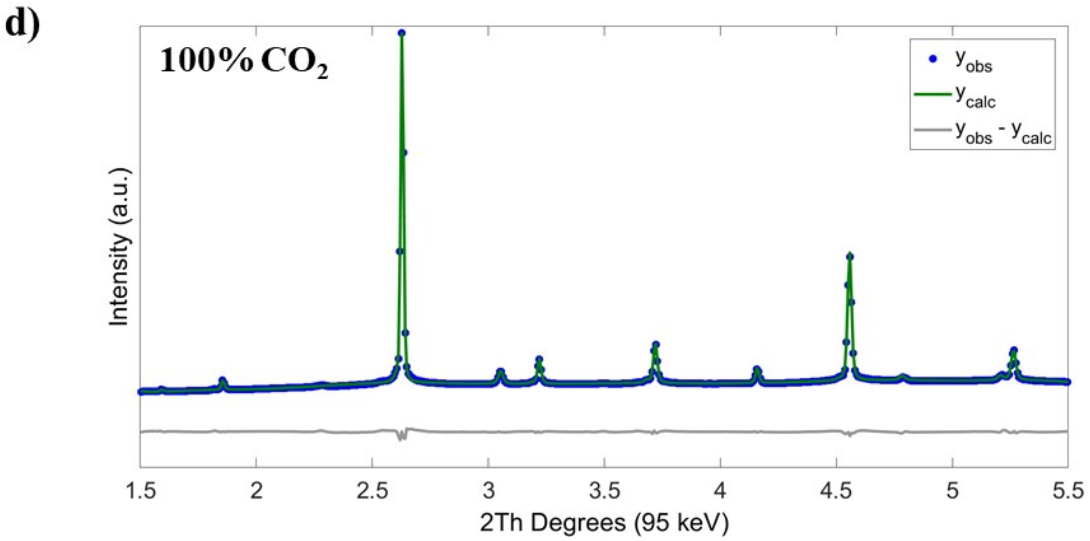

Figure S17. Fits from the full profile analysis of the mean diffraction patterns from four selected XRD-CT datasets from the first CMR experiment: a) scan at room temperature of the fresh membrane, b) scan at high temperature after Ar treatment, c) second scan under OCM reaction conditions and d) scan under 100 % CO_2.

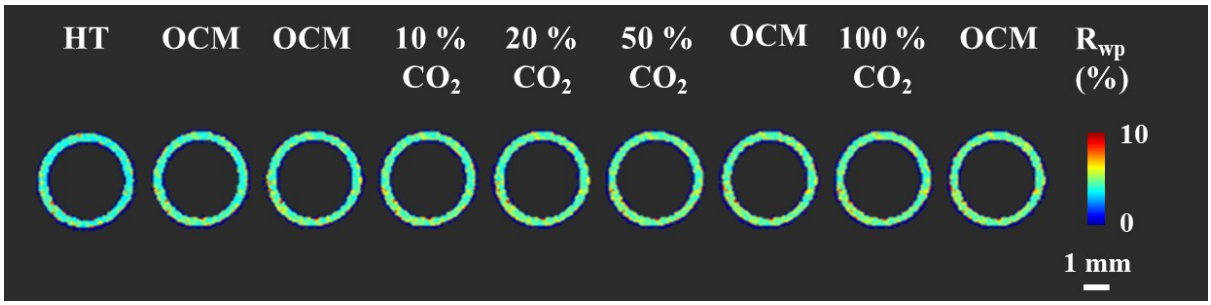

Figure S18. Distribution of Rwp for all high temperature XRD-CT measurements. The error is both very low and uniform for all XRD-CT datasets.

S5. Laboratory measurements

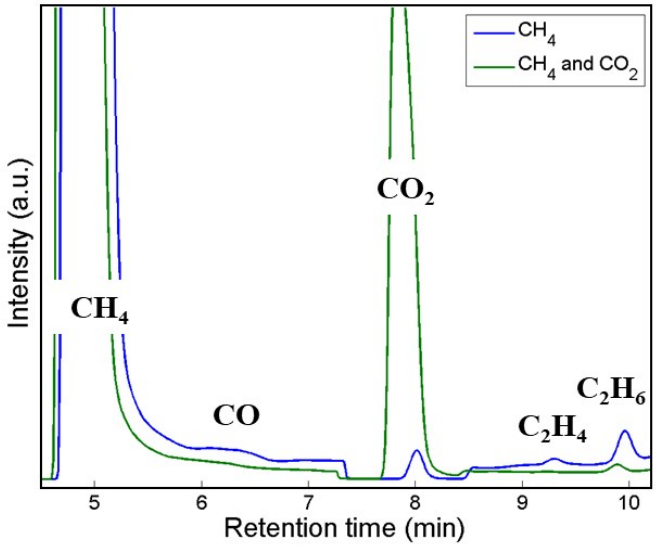

Figure S19. Results of gas chromatography analysis during the OCM measurements with membrane-only CMR. The presented graphs compare the analysis of outflow gases for OCM reaction mixtures containing CH_4 (blue) and CO_2 and CH_4 (green).

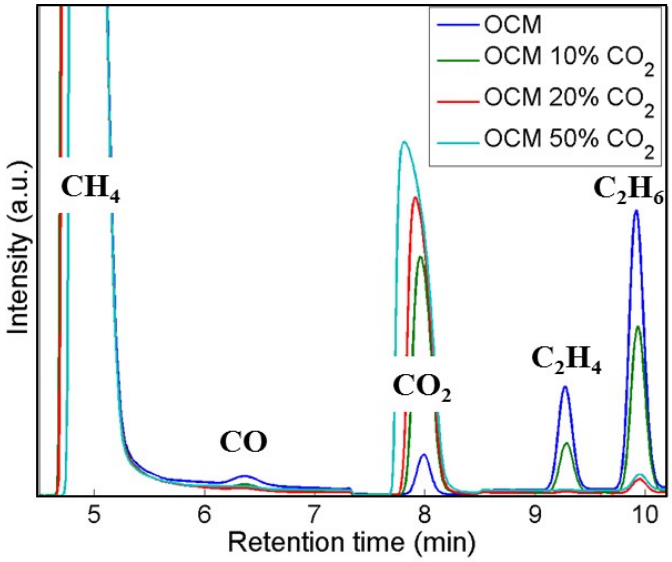

Figure S20. Results of gas chromatography analysis during the OCM measurements with packed-bed CMR. The presented graphs compare the analysis of outflow gases for OCM reaction mixture with different quantity of CO_2.

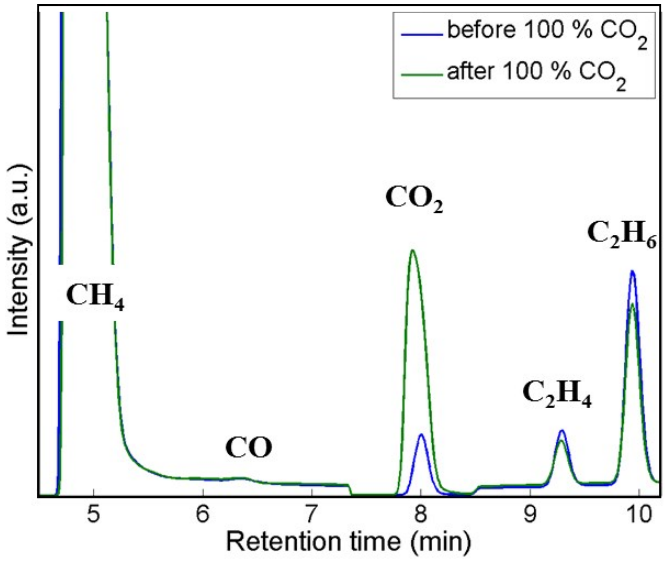

Figure S21. Results of gas chromatography analysis during the OCM measurements with packed-bed CMR. The presented graphs compare the analysis of outflow gases for OCM reaction mixture before and after treatment of the system in pure CO_2.

S6. SEM/EDX measurements

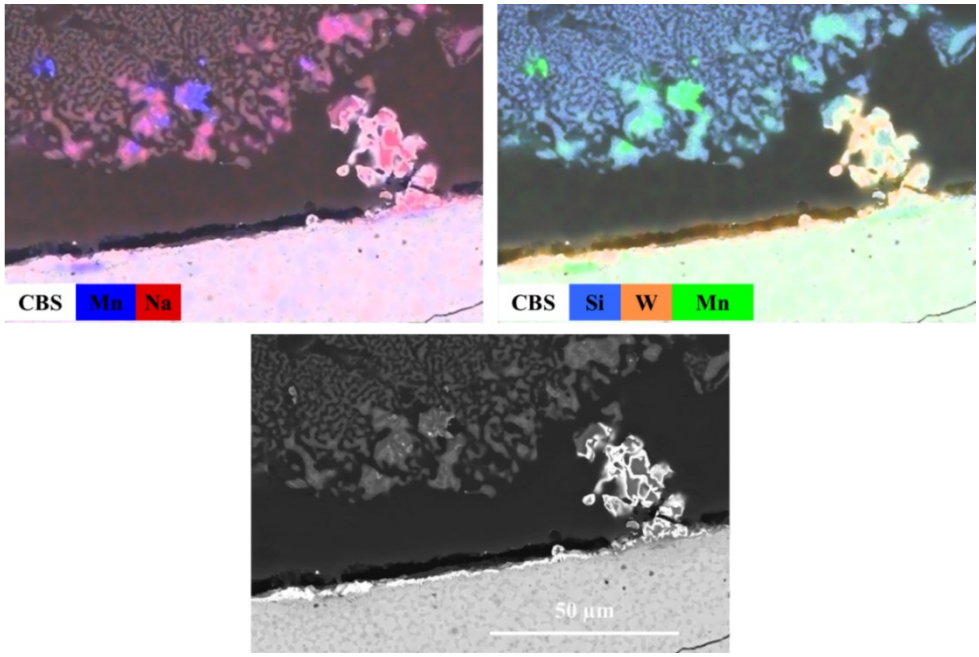

Figure S22. Elemental distribution of components in catalyst particles and at the inner side of membrane obtained by EDX mapping. This fragment of the membrane cross section was obtained from the reactor inlet.